Catalysis Today 147 (2009) 62–67

Contents lists available at ScienceDirect

Catalysis Today

journal homepage: www.elsevier.com/locate/cattod

A comparative study of methanol carbonation on unsupported SnO_2 and ZrO_2

Daniel Aymes [a], Danielle Ballivet-Tkatchenko [b,*], Kulandailevu Jeyalakshmi [b], Lucien Saviot [a], Sivakumar Vasireddy [b,1]

[a] Université de Bourgogne et CNRS, UMR 5209, Institut Carnot de Bourgogne, F-21000 Dijon, France
[b] Université de Bourgogne et CNRS, UMR 5260, Institut de Chimie Moléculaire, F-21000 Dijon, France

ARTICLE INFO

Article history:
Available online 31 July 2009

Keywords:
Methanol
Dimethyl carbonate
Carbon dioxide
Nanoparticles
Tin oxide
Zirconium oxide

ABSTRACT

The aim of this work was to explore the catalytic properties of SnO_2 in the coupling of methanol with carbon dioxide to afford dimethyl carbonate. SnO_2 nanopowders were produced by hydrolysis of tin tetra-*tert*-butoxide dissolved in *n*-butanol. The samples were much more active than a commercial one due to their higher surface areas. In addition, they exhibited excellent recyclability. However, comparison with ZrO_2, prepared and tested under the same experimental conditions, showed that zirconia-based catalysts were more selective and are, among the heterogeneous catalysts already reported, still the more selective. SnO_2 also catalyzed the formation of dimethyl ether likely due to lower rates in the formation of the key intermediate $CH_3OC(O)O$–Sn and its subsequent alkylation by activated methanol. This lack of selectivity contrasts with that of soluble organotin(IV) which are totally selective to DMC formation. Structural characterization of SnO_2 was performed by X-ray powder diffraction, laser Raman spectroscopy, transmission electron microscopy, and nitrogen isotherm. As found from X-ray diffraction line broadening, the crystallite size of all powders was in the nanometric range (cassiterite structure) which was confirmed by transmission electron microscopy. Moreover, the low-frequency Raman scattering allowed to determine an average particle size diameter of 4 nm.

1. Introduction

In recent years methanol is receiving much attention for developing alternative technologies in the energy sector [1]. But still its current major application is in the chemical sector. Considering the stimulative context of non-fossil carbon resources for making organics, coupling methanol with CO_2 presents the unique advantage of utilizing only CO_2 as carbon feedstock, provided methanol is thereof obtained by hydrogenation [2–4]. One of the challenging targets is dimethyl carbonate (DMC) [5,6]. DMC finds applications ranging from organic synthesis [7] and phosgene-free synthesis of polymers [8] to gasoline blending [9]. Interestingly enough, DMC has low toxicity, rapid biodegradability [8] and low impact on air quality [10]. However, its scale-up production based on the on-stream technologies is limited due to intrinsic constraints of the processes [11,12]. Therefore, its synthesis from CO_2 and methanol according to reaction (1) is highly attractive.

$$2CH_3OH + CO_2 \rightleftharpoons DMC + H_2O \quad (1)$$

The current main issue is to enhance the rate and conversion of methanol. One option has been demonstrated in adding water traps to the catalytic systems for preventing catalyst deactivation by water as well as to shifting the equilibrium [13,14]. Nevertheless, there is a need for exploring new catalysts and understanding the reaction mechanism for rate enhancement in the absence of water trap additives. In recent years, a variety of heterogeneous catalysts have been screened under different *P*–*T* reaction conditions. The reaction is commonly run under high pressure, 100–300 bar, at 130–180 °C over ZrO_2 [15–17], H_3PO_4/ZrO_2 [18], CeO_2 [19], mixed ZrO_2–CeO_2 [20], polyoxometalates [21], supported copper (Ni, V, O) [22], copper–nickel/graphite [23], and V-doped Cu–Ni/AC catalysts [24]. Among the catalysts studied, zirconia-based are still those exhibiting the highest selectivity to DMC (~100%). A thorough understanding of the reaction mechanism shows that surface Zr–OH groups and $Zr^{4+}O^{2-}$ sites act as Lewis acid–base pairs for the bifunctional activation of methanol. The insertion of CO_2 into the CH_3O–Zr bond to form hemicarbonate $CH_3OC(O)O$–Zr species is the key elementary step

* Corresponding author at: Université de Bourgogne et CNRS, UMR 5260, Institut de Chimie Moléculaire, BP 47870, F-21000 Dijon, France. Tel.: +33 3 80 39 37 70; fax: +33 3 80 39 37 72.
E-mail address: ballivet@u-bourgogne.fr (D. Ballivet-Tkatchenko).
[1] Present address: Department of Chemical Engineering, Louisiana State University, South Stadium Drive, Baton Rouge, LA 70803, United States.

0920-5861/$ – see front matter © 2009 Elsevier B.V. All rights reserved.
doi:10.1016/j.cattod.2009.07.001

[17,18]. Subsequent fast methyl transfer to $CH_3OC(O)O$–Zr from CH_3OH activation on acid sites likely occurs for getting the high selectivity to DMC. During the processes of methanol activation, the concomitant formation of water may induce CH_3O–Zr hydrolysis, therefore leading to a decrease in catalyst activity.

Interestingly enough, organometallic complexes such as diorganotin(IV) compounds are also active precursors and, importantly, totally selective [14,25–27]. The reversible insertion of CO_2 into the CH_3O–Sn bond of dialkyldimethoxystannanes has been evidenced which accounts for the need of high CO_2 pressure under catalytic conditions. Nonetheless, the corresponding complexes bearing the hemicarbonate $CH_3OC(O)O$–Sn moiety have been isolated and structurally characterized [26,28]. This result stresses on the similarity of reaction events on both types of catalysts for this particular reaction. Concerning the tin species involved in the catalytic cycle, we could very recently isolate during the course of the reaction multinuclear dibutyloxocarbonato tin(IV) intermediates, that play a key role in the process. Their structure elucidation by single-crystal X-ray diffraction allows to view these species as organo-oxides [29,30]. It was therefore tempting to look at the catalytic behavior of SnO_2 to screen for the impact of ligand-free catalytic sites on their activity and selectivity for DMC synthesis. To the best of our knowledge, there is only one report in a patent on the relevant catalytic behavior of SnO_2, but the reaction selectivity was not reported [13].

We herein report the catalytic performance of SnO_2 with emphasis on DMC yield with reaction time and recyclability of the catalyst. The synthesis of SnO_2 was achieved by a free-chloride sol–gel route from tin tetra-*tert*-butoxide. The prepared catalysts were characterized by X-ray powder diffraction (XRD), laser Raman spectroscopy, transmission electron microscopy (TEM) and nitrogen isotherm for determining the crystalline phase, grain size, and morphology. ZrO_2 was also prepared, on purpose, by the same method to get a reference under our reaction conditions as it exhibits the highest selectivity among the heterogeneous catalysts reported so far.

2. Experimental

2.1. General

All manipulations were carried out under argon by using standard Schlenk techniques. Methanol (Carlo Erba, RPE grade) was dried and distilled from $Mg(OCH_3)_2$, *tert*-butanol (Fluka, >99%) and *n*-butanol (Fluka, >98%) dried over 3 Å molecular sieves. Deionized water was refluxed for 2 h prior to use. Carbon dioxide N45 TP purchased from Air Liquide was used without further purification. Tin tetra-*tert*-butoxide was synthesized from $SnCl_4$ (Aldrich, 99%) according to a published procedure [31]. Zirconium tetra-*n*-butoxide (80 wt% *n*-BuOH solution, Aldrich) was used without further purification. A commercial nanopowder of tin(IV) oxide from Aldrich was used for comparison.

2.2. Synthesis of SnO_2 and ZrO_2

Tin and zirconium oxides were synthesized by hydrolysis of $Sn(O^tBu)_4$ and $Zr(O^nBu)_4$, respectively. The afforded white powders were obtained with yields >90%, based on the starting alkoxides. In a typical experiment, a *n*-butanol solution (100 ml) of $Sn(O^tBu)_4$ (25 g, 0.06 mol) was added dropwise over 5 h under vigorous stirring to deionized water (600 ml) maintained at 15 °C. The slurry was kept stirring for 1 h, then overnight for settling, and finally subjected to centrifugation with a Biofuge Startos Heraeus apparatus. The solid was washed with distilled water and submitted to lyophilisation overnight (FTS systems, EZDRY). Analysis for residual carbon was performed at the Institut de Chimie Moléculaire de l'Université de Bourgogne, Dijon. All samples have C content <0.2%.

2.3. Catalyst characterization

X-ray powder diffraction (XRD) patterns were collected with a Siemens D5000 diffractometer using Cu-Kβ (λ = 0.139222 nm) radiation.

Transmission electron microscopy (TEM) was performed using a JEOL JEM-2100 microscope at 200 kV accelerating voltage. Sample preparation consisted in dispersing the SnO_2 powder in ethanol under sonication, then dropping the dispersion on a copper grid coated with amorphous carbon membrane.

The Raman spectra were obtained at room temperature using a Jobin-Yvon T64000 spectrometer coupled to an Olympus microscope. Excitation was provided by an Ar laser operating at 514.5 nm. The laser power was kept as low as possible to prevent local heating. The resolution of the spectrometer was 1 cm^{-1}.

Nitrogen sorption data were obtained at −196 °C with a BELSORP-mini apparatus after outgassing the samples at 100 °C for 12 h. The specific surface area (SSA) was calculated from the BET method.

Thermogravimetric analysis (TGA) was performed with a Setaram TAG 24 system at a heating rate of 1 °C min^{-1} to 500 °C under N_2–O_2 atmosphere (N_2:O_2 = 75:25; flow rate, 0.15 mL min^{-1})

2.4. Catalytic experiments

Caution: since high pressures are involved, appropriate safety precautions must be taken.

The catalysts (0.100–0.550 g) were pretreated under vacuum at 120 °C for 2 h, then 20 ml of dried methanol was added. The suspension was transferred under argon into a 120-ml batch stainless steel autoclave, followed by the admission of either 40 or 20 g of CO_2 with an ISCO 260D pump to get a working pressure of either 200 or 120 bar. The autoclave was heated to 150 °C (controlled by an internal K-thermocouple). After a given reaction time, the autoclave was cooled down to 0 °C, pressure gently released through a valve, and the liquid phase transferred for GC analysis with a Fisons 8000 apparatus (FID detector, toluene as internal standard, column: J&W Scientific DB-WAX 30 m capillary column). Identification of the products was done by GC–MS (Fisons MD800, J&W Scientific DB-5MS 60 m capillary column). For recycling experiments, the catalyst was recovered by centrifugation, then pretreated at 120 °C for 2 h under vacuum, loaded into the autoclave following the aforementioned procedure. DMC yield was also analyzed as a function of time during the course of the reaction by sampling with a high pressure valve. At the end of such experiments, degassing the autoclave at 0 °C followed by GC analysis of the liquid phase allowed to check consistency between the two procedures; the fit was better than 3% (relative error).

3. Results and discussion

3.1. DMC synthesis from methanol and CO_2

All catalytic tests were performed at 150 °C under CO_2 pressure in a batch autoclave. The working pressure was set at either 120 or 200 bar. These values were chosen for their relevance to two different domains in the fluid phase diagrams of the MeOH/CO_2 binary mixtures herein used [29]. With *P*–*T* conditions of 120 bar–150 °C, the reacting mixture is a two-phase liquid–vapor consisting in methanol-rich liquid and CO_2-rich vapor phases. At 200 bar–150 °C, the reactants are totally miscible, thus forming a single supercritical phase. Switching from biphasic to monophasic conditions induces changes in reactant concentration, adsorp-

tion–desorption equilibrium at catalyst surface and fluid density, playing therefore an important role on the course of the reaction [32]. Such a fluid phase equilibrium effect has been clearly identified on the DMC yield with soluble catalysts [33].

Preliminary screening with commercial SnO_2 nanopowder (SSA = 40 $m^2\ g^{-1}$) showed a negligible activity. As the catalytic activity might be related to the surface area, the synthesis of SnO_2 powders was, therefore, undertaken with the objective of getting much higher surface areas. A sol–gel procedure from tin tetra-*tert*-butoxide was successfully applied for getting several batches of about 10 g with SSA ranging from 140 to 190 $m^2\ g^{-1}$, respectively. Two of those batches (140 and 170 $m^2\ g^{-1}$) were used in this study. In the following, the corresponding samples will be identified as SnO_2(140) and SnO_2(170). After a pretreatment under vacuum at 120 °C, the obtained powders did catalyze significantly DMC formation. For comparison, ZrO_2 powders were also synthesized according to the same procedure. Three batches were obtained with SSA of 80, 155 and 172 $m^2\ g^{-1}$, respectively. In order to optimize the amount of catalyst in each run, DMC yield was first evaluated versus catalyst weight in the range 0.100–0.550 g (Fig. 1A). The linear relationship obtained for SnO_2 as well as for ZrO_2 indicates that the reaction is kinetically controlled. Moreover, the conversion into DMC was found to increase linearly with SSA values of both oxides (Fig. 1B), a correlation which has been noticed previously on ZrO_2 and CeO_2/ZrO_2 mixed oxides [24,25]. Fig. 1B also reveals that tin(IV) oxide activity is ~40% that of zirconia.

Fig. 2 reports the kinetics of DMC formation over ZrO_2 and SnO_2, at 150 °C under 120 and 200 bar. In the case of ZrO_2, the DMC yield increases steadily for several hours of reaction before reaching a plateau. The selectivity for DMC was found to be close to 100%. During the first 6 h of a run, DME was under the detection limit but analyzed in trace amounts at longer reaction times. Pressure effect, 120 or 200 bar, is not apparent during the increase of DMC yield. This behavior is tentatively assigned to the inverse relationship between methanol and CO_2 concentrations when comparing biphasic (120 bar) and monophasic (200 bar) conditions. Because the amount of methanol introduced in the batch reactor of constant volume was the same for both experiments, the biphasic regime leads to a liquid methanol-rich phase of smaller volume than where methanol forms a monophasic supercritical phase with CO_2 that occupies the entire volume of the reactor. On the other hand, the amount of CO_2 charged into the reactor was greater at higher pressure, i.e. monophasic conditions. Therefore, the pressure effect on the kinetics may be somehow neutralized. Conversely, the pressure effect is evidenced at the plateau, corresponding to a methanol conversion of 0.7% and 0.4% at 200 and 120 bar, respectively. Crosschecking allowed to discard thermodynamic equilibrium-controlled conversion. Hence, it seems plausible that poisoning of the active sites may occur by coproduced water (Eq. (1)). Indeed, the activity was restored after ex-situ thermal reactivation of the catalysts. The lower value of the plateau observed under biphasic conditions may be assigned to the increase in water concentration as water has high affinity for the liquid methanol-rich phase due to the protic nature of alcohols.

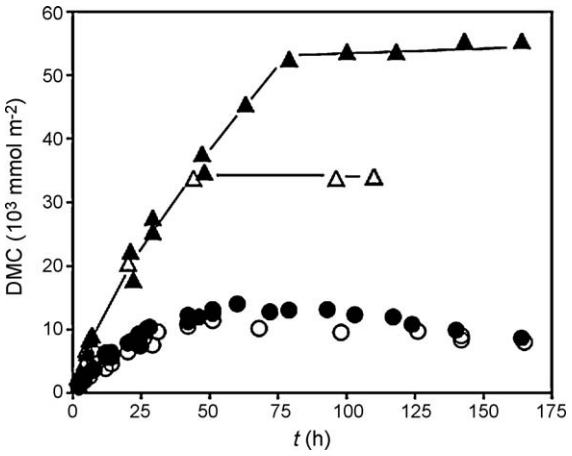

Fig. 2. DMC yield as a function of reaction time and pressure at 150 °C on SnO_2 ((●) 200 bar and (○) 120 bar) and ZrO_2 ((▲) 200 bar and (△) 120 bar).

Interestingly, the signature of SnO_2 catalyst is quite different (Fig. 2). First, the rate of DMC formation is slower than over ZrO_2. Second, the observed plateau after 50 h run is not markedly pressure dependent. As a matter of fact, the reaction was found to be non-selective in DMC. The other product was identified as dimethyl ether (DME) by GC–MS analysis. An experimental setup for on-line analysis of the reaction mixture allowed to determine DMC selectivity with reaction time. As shown in Fig. 3, DME is steadily increasing during a 175-h run, whereas DMC formation ceased after 75 h. The shape of the two curves suggests the occurrence of parallel reactions from methanol, i.e. dehydration

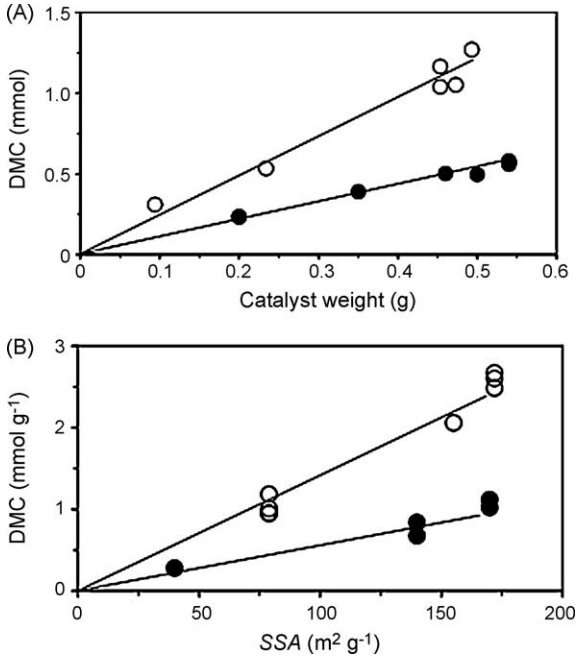

Fig. 1. DMC yield as a function of catalyst weight (A) and catalyst surface area (B) at 150 °C and 200 bar for 14 h on (●) SnO_2(170) and (○) ZrO_2(172).

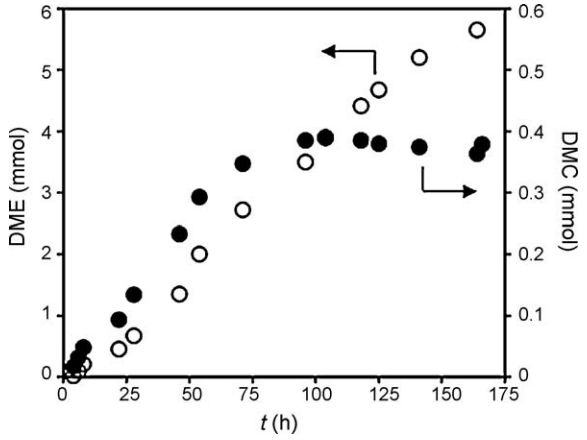

Fig. 3. DMC (●) and DME (○) yields as a function of time on SnO_2(140) at 150 °C and 200 bar.

and carbonation, instead of successive carbonation of methanol to DMC followed by decomposition into DME. Hence, water produced by methanol dehydration to DME likely contributes to the decrease in the rate of DMC formation. From this it is inferred that the extent of surface hydroxylation, or hydration, influences the nature and concentration of the relevant adsorbed species. In particular, adsorbed methoxy species are unstable under hydrolytic conditions giving back methanol. Hence, the concentration of the key hemicarbonate intermediate, CH_3O-C(O)O–M (M = Zr, Sn), characterized over ZrO_2 [17,18] and with organometallic tin derivatives [26,28] is decreased. The occurrence of methanol dehydration to DME suggests that the reaction of $CH_3OC(O)O$–Sn with methanol to afford DMC is not as fast as in the case of the ZrO_2-based systems. On the basis of the structural characterization reported in the following, further work is in progress for tuning the SnO_2 surface sites.

In order to examine the stability and deactivation of the catalysts, recycling experiments were undertaken according to the following procedure. After the first run, the catalyst was recovered by centrifugation, outgassed at 120 °C for 2 h, then re-used. On ZrO_2, after four recyclings with each reaction time of 14 h the DMC yield remains constant. Extensive recyclings were undertaken with SnO_2 with pressure changes, 200 or 120 bar, as well as reaction time changes, from 12 to 60 h. Again, the DMC yield remains practically unchanged. Cumulative recyclings corresponding to 17 days of reaction on SnO_2(170) led to a slight decrease of SSA down to 145 $m^2\ g^{-1}$. This sample will be denoted as used-SnO_2(170) in the characterization part which follows in this paper. Thus, it can be concluded that the catalysts exhibit excellent stability at the lab scale.

3.2. Catalyst characterization

The structural properties of the prepared SnO_2 were determined by XRD, TEM, Raman spectroscopy, N_2 adsorption–desorption, and TGA to determine the crystalline phase, grain size, and morphology.

Fig. 4 shows the XRD patterns of SnO_2(170), used-SnO_2(170), and SnO_2 from commercial source. The samples were pretreated under vacuum at 120 °C for 2 h. All reflections are in excellent accordance with a tetragonal rutile structure (JCPDS Card No. 41-1445). The measured peaks are relatively wide for the SnO_2(170) and used-SnO_2(170) samples indicating that the crystal size is very small (patterns a and b). Peak overlapping prevented a careful determination of the crystallite size. Instead a different method, Raman spectroscopy, was used which provided information not only on the average size but also on the size distribution of the grains. The XRD peaks for commercial SnO_2 (pattern c) are much narrower due to bigger crystallite size in agreement with the low-frequency Raman spectrum above described.

TEM observations match with the XRD signature of small crystallites. The corresponding TEM bright-field imaging of SnO_2(170) shows a loose aggregation of uniformly distributed pseudo-spherical grains of 5 nm as average diameter (Fig. 5A). Nanocrystals may be distinguished in the dark-field observation mode (Fig. 5B).

More evidence on the formation of nano-SnO_2 came from the Raman spectral signature in the low-frequency region (<150 cm^{-1}), which changes drastically with the size of the particles. The confinement of acoustic vibrations in nanoscale particles results in an additional peak, the position of which vary as the inverse diameter [34]. Using the directionally averaged sound velocities, longitudinal 6530 m/s and transverse 3120 m/s, taken from Ref. [35], we obtain $\omega = 193.2/d$ where ω is the frequency of the breathing mode expressed in cm^{-1} and d the diameter of the SnO_2 sphere in nm. These vibrations are hardly damped in the case of a powder because the contact between nanoparticles is poor. Therefore, the width of the low-frequency peak reflects the size and shape distribution [36]. Assuming that the nanoparticles are mostly spherical, as shown by TEM, and taking into account the variation of the electron–phonon coupling with the diameter of the nanoparticle [37], the size distribution can be obtained from the shape of the low-frequency peak. Fig. 6A reports the low-frequency spectra for three

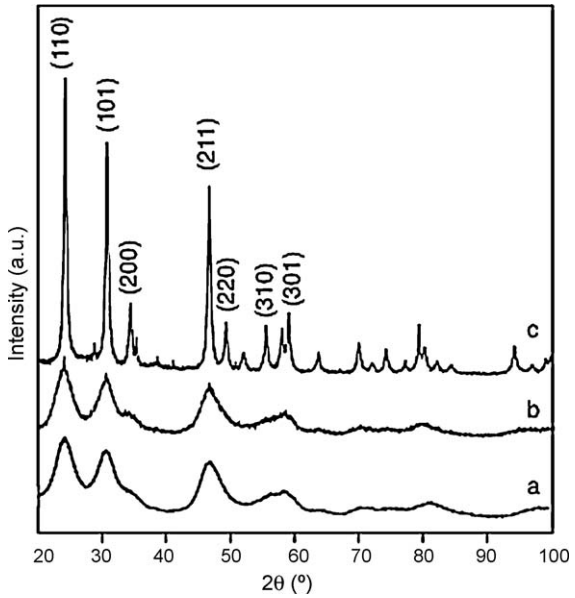

Fig. 4. XRD patterns of SnO_2 samples pretreated under vacuum at 120 °C: (a) SnO_2(170), (b) used-SnO_2(170) and (c) commercial sample.

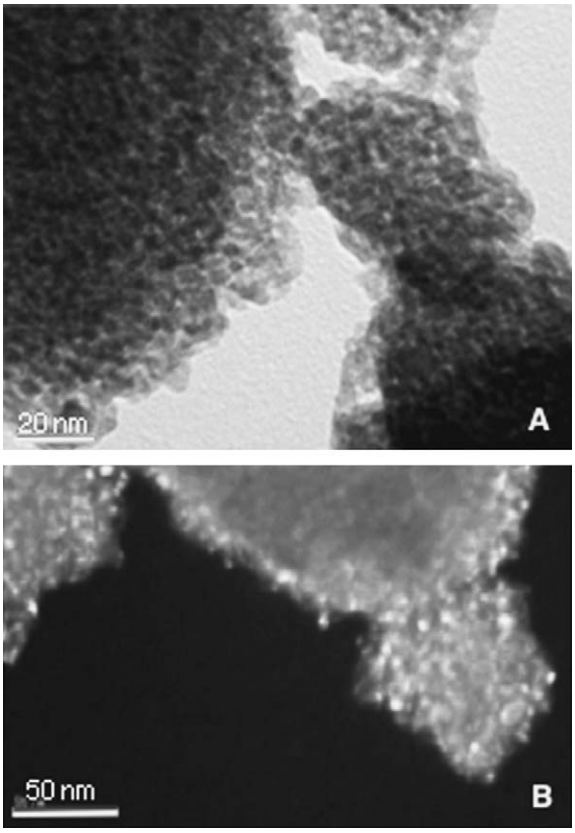

Fig. 5. TEM images of SnO_2(170) pretreated under vacuum at 120 °C: (A) bright field and (B) dark field.

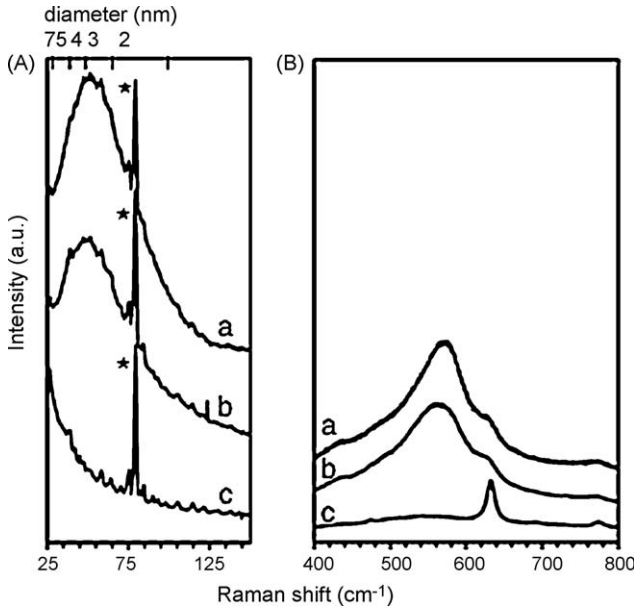

Fig. 6. Enlarged view of Raman spectra of SnO_2 samples pretreated under vacuum at 120 °C: (a) SnO_2(170), (b) used-SnO_2(170) and (c) commercial sample. (A): (★) plasma lines, secondary *x*-axis for diameter scale.

SnO_2 samples, SnO_2(170), used-SnO_2(170) and commercial SnO_2. The secondary *x*-axis gives the diameter scale calculated from the aforementioned equation. The SnO_2(170) and used-SnO_2(170) samples exhibit one broad band characterized by a maximum at ca. 4 nm and a half-width of about 2–2.5 nm. The commercial sample does not present any band in the low-frequency region due to particle size >7 nm.

Apart from the low-frequency scattering, the Raman spectra contain peaks associated to the optical modes of the rutile structure as well as additional disorder activated contributions as reported elsewhere [36]. Because the diameter of the nanoparticles is quite small in this study, the scattering by optical modes is not very intense. Nevertheless, in the 500–650 cm^{-1} range one can easily distinguish two bands (Fig. 6B). A broad band at 570 cm^{-1} features surface stretching Sn–O vibration modes while the narrower one at 632 cm^{-1} appears in bulk polycrystalline SnO_2 [38]. Interestingly, the broad band is only present on SnO_2(170) and used-SnO_2(170) samples that exhibit a small size distribution as determined from the low-frequency region. This result points out a high surface/volume ratio for the prepared SnO_2 samples.

The corresponding N_2 adsorption–desorption isotherms for SnO_2(170) and used-SnO_2(170) samples are of type I (IUPAC classification) indicating main microporosity. A minor mesoporosity was evidenced by the hysteresis loop at $0.4 < p/p_o < 0.6$, that may be ascribed to inter-crystallite porosity due to agglomeration as shown by TEM image (Fig. 4a). Noteworthy, the shape of the sorption isotherm remains unchanged on the used-SnO_2(170) sample. The slight decrease observed in the adsorption capacity fits with the decrease in the SSA value: 146 $m^2 g^{-1}$ vs 170 $m^2 g^{-1}$. Hence, the large SSA values are due to small crystal size. On such solids, the mean diameter, *d*, of the crystallites can be estimated from the SSA value, assuming spherical grains. The corresponding equation, $d\ (nm) = 6 \times 10^3/(6.95)(SSA)$, provides average *d* values of 5 and 6 nm, respectively, that are close to those found by Raman experiments.

Thermogravimetric analysis under air of SnO_2(170) sample showed two steps for weight loss. The first step below 75 °C corresponds to about 10% weight loss, whereas the second one from 160 to 500 °C accounts for 15%. A discontinuity was observed between 90 and 160 °C that features two successive dehydration steps assigned to molecular water desorption then to dehydroxylation [39]. Therefore, under our pretreatment conditions for catalytic experiments (120 °C) the surface of the SnO_2 samples can be seen as extensively hydroxylated.

4. Conclusion

Our results show that SnO_2 prepared by the sol–gel route from $Sn(O^tBu)_4$ is active in the coupling of methanol with CO_2 to DMC. Comparison with ZrO_2, prepared and tested under the same conditions, highlights that, among the heterogeneous catalysts studied, zirconia-based catalyst is still the reference for high DMC selectivity. DMC yield increases linearly with SSA of both oxides, but SnO_2 is also active in methanol dehydration to DME. High selectivity to DMC has been previously assigned to fast elementary processes that convert methoxy to the hemicarbonate species, $CH_3OC(O)O$–M, under high CO_2 pressure, followed by alkylation from activated methanol on acidic sites. Interestingly enough, a similar reaction pathway has been already demonstrated with organotin(IV) complexes that are totally selective to DMC. Structural characterization of SnO_2 shows that the synthetic procedure leads to the formation of microporous nanosized grains of 4 nm as mean diameter, promoting high SSA value. Moreover, the low-frequency Raman signature allows to calculate the grain size distribution. The nanoparticles thus far obtained are extensively recyclable which offers an attractive alternative to soluble organotin(IV) catalysts provided the selectivity issue can be overcome in fine tuning of the SnO_2 surface sites.

Acknowledgements

Financial support from CNRS and the Fédération de recherche "Caractérisation et Technologie de la Matière" are greatly acknowledged. S.V. and K.J. thank the Conseil Régional de Bourgogne for postdoctoral grants. The authors also wish to warmly thank Dr. N. Millot for TEM experiments.

References

[1] G.A. Olah, Angew. Chem. Int. Ed. 44 (2005) 2636.
[2] C. Song, Catal. Today 115 (2006) 2.
[3] G. Zahedi, A. Elkamel, A. Lohi, A. Jahanmiri, M.R. Rahimpor, Chem. Eng. J. 115 (2005) 113.
[4] E. Vesselli, L. De Rogatis, X. Ding, A. Baraldi, L. Savio, L. Vattuone, M. Rocca, P. Fornasiero, M. Peressi, A. Baldereschi, R. Rosei, G. Comelli, J. Am. Chem. Soc. 130 (2008) 11417.
[5] T. Sakakura, J.-C. Choi, H. Yasuda, Chem. Rev. 107 (2007) 2365.
[6] M. Aresta, A. Dibenedetto, Dalton Trans. (2007) 2975.
[7] P. Tundo, M. Selva, Acc. Chem. Res. 35 (2002) 706.
[8] F. Rivetti, C. R. Acad. Sci. Paris Chem. 3 (2000) 497.
[9] M.A. Pacheco, C.L. Marshall, Energy Fuels 11 (1997) 2.
[10] Y. Katrib, G. Deiber, P. Mirabel, S. Le Calve, C. George, A. Mellouki, G. Le Bras, J. Atmos. Chem. 43 (2002) 151.
[11] S. Uchiumi, K. Ataka, T. Matsuzaki, J. Organomet. Chem. 576 (1999) 279.
[12] D. Delledonne, F. Rivetti, U. Romano, Appl. Catal. A 221 (2001) 241.
[13] A. Wagner, W. Haas, WO/1994/022805 (1994).
[14] T. Sakakura, J.-C. Choi, Y. Saito, T. Masuda, T. Sako, T. Oriyama, J. Org. Chem. 64 (1999) 4506.
[15] K. Tomishige, T. Sakaihori, Y. Ikeda, K. Fujimoto, Catal. Lett. 58 (1999) 225.
[16] S. Xie, A.T. Bell, Catal. Lett. 70 (2000) 137.
[17] K.T. Jung, A.T. Bell, J. Catal. 204 (2001) 339.
[18] Y. Ikeda, M. Asadullah, K. Fujimoto, K. Tomishige, J. Phys. Chem. B 105 (2001) 10653.
[19] Y. Yoshida, Y. Arai, S. Kado, K. Kunimori, K. Tomishige, Catal. Today 115 (2006) 95.
[20] K. Tomishige, Y. Furusawa, Y. Ikeda, M. Asadullah, K. Fujimoto, Catal. Lett. 76 (2001) 71.
[21] C. Jiang, Y. Guo, C. Wang, C. Hu, Y. Wu, E. Wang, Appl. Catal.: Gen. 256 (2003) 203.
[22] X.J. Wang, M. Xiao, S.J. Wang, Y.X. Lu, Y.Z. Meng, J. Mol. Catal. A: Chem. 278 (2007) 92.
[23] J. Bian, M. Xiao, S. Wang, X. Wang, Y. Lu, Y. Meng, Chem. Eng. J. 147 (2009) 287.
[24] J. Bian, M. Xiao, S. Wang, Y. Lu, Y. Meng, Catal. Commun. 10 (2009) 1142.
[25] J. Kizlink, I. Pastucha, Collect. Czech. Chem. Commun. 60 (1995) 687.
[26] D. Ballivet-Tkatchenko, O. Douteau, S. Stutzmann, Organometallics 19 (2000) 4563.

[27] D. Ballivet-Tkatchenko, T. Jerphagnon, R. Ligabue, L. Plasseraud, D. Poinsot, Appl. Catal. A: Gen. 255 (2003) 93.
[28] J.-C. Choi, T. Sakakura, T. Sako, J. Am. Chem. Soc. 121 (1999) 3793.
[29] D. Ballivet-Tkatchenko, S. Chambrey, R. Keiski, R. Ligabue, L. Plasseraud, P. Richard, H. Turunen, Catal. Today 115 (2006) 80.
[30] D. Ballivet-Tkatchenko, R. Burgat, S. Chambrey, L. Plasseraud, P. Richard, J. Organomet. Chem. 691 (2006) 1498.
[31] M.J. Hampden-Smith, T.A. Wark, A. Rheingold, J.C. Huffman, Can. J. Chem. 69 (1991) 121.
[32] M. Nunes da Ponte, J. Supercrit. Fluids 47 (2009) 344.
[33] Z. Hou, B. Han, Z. Liu, T. Jiang, G. Yang, Green Chem. 4 (2002) 467.
[34] E. Duval, A. Boukenter, B. Champagnon, Phys. Rev. Lett. 56 (1986) 2052.
[35] R.S. Katiyar, P. Dawson, M.M. Hargreave, G.R. Wilkinson, J. Phys. C 4 (1971) 2421.
[36] A. Dieguez, A. Romano-Rodriguez, J. Ramon Morante, N. Barsan, U. Weimar, W. Gopel, Appl. Phys. Lett. 71 (1997) 1957.
[37] C. Pighini, D. Aymes, N. Millot, L. Saviot, J. Nanopart. Res. 9 (2007) 309.
[38] L. Abello, B. Bochu, A. Gaskov, S. Koudryavtseva, G. Lucazeau, M. Roumyantseva, J. Solid State Chem. 135 (1998) 78.
[39] P.G. Harrison, A. Guest, J. Chem. Soc., Faraday Trans. 1 (83) (1987) 3383.